NACA

RESEARCH MEMORANDUM

TURBULENT CONVECTIVE HEAT-TRANSFER COEFFICIENTS MEASURED FROM FLIGHT TESTS OF FOUR RESEARCH MODELS (NACA RM-10) AT MACH NUMBERS FROM 1.0 TO 3.6

By Leo T. Chauvin and Joseph P. Maloney

Langley Aeronautical Laboratory
Langley Field, Va.

NATIONAL ADVISORY COMMITTEE
FOR AERONAUTICS

WASHINGTON
March 11, 1955

NATIONAL ADVISORY COMMITTEE FOR AERONAUTICS

RESEARCH MEMORANDUM

TURBULENT CONVECTIVE HEAT-TRANSFER COEFFICIENTS MEASURED FROM FLIGHT TESTS OF FOUR RESEARCH MODELS (NACA RM-10) AT MACH NUMBERS FROM 1.0 TO 3.6

By Leo T. Chauvin and Joseph P. Maloney

SUMMARY

Convective heat-transfer coefficients have been evaluated from skin temperatures measured along the body of a research model designated NACA RM-10. The general shape of the body is a parabola of revolution of fineness ratio 12.2.

Heat-transfer data are presented for a Mach number range of 1.0 to 3.6 and for a Reynolds number range of 6×10^6 to 150×10^6 based on axial distance from the nose to the point at which the temperature measurements were made.

The heat-transfer data are presented as the Nusselt number divided by the cube root of the Prandtl number, expressed as a function of Reynolds number. The data from four flight tests are in agreement with the equation for turbulent heat-transfer measurements which was derived from previous flight tests of two RM-10 models.

The heat transfer is also correlated with a compressible-flow theory for turbulent heat transfer which uses the boundary-layer thickness as the length parameter in the Nusselt and Reynolds numbers. The data were also in agreement with this theory.

The measured recovery factors were lower than those predicted by theory for turbulent boundary layer.

The relationship of heat transfer to skin friction was investigated by comparing the heat transfer of the present investigation with the measured skin-friction results obtained from additional flight tests of this model.

INTRODUCTION

The theory of aerodynamic heating for a turbulent boundary layer at supersonic speeds is as yet in its formative stage. A need exists for experimental measurements under full-scale, free-flight conditions to aid in the development of theory as well as provide design data for supersonic airplanes and guided missiles. Most experimental heat-transfer investigations have been done in wind tunnels utilizing steady-state conditions and low stagnation temperatures (for example, refs. 1 and 2); however, some experimental work has been done in free flight for transient condition along a trajectory (for example, refs. 3 and 4). Flight tests provide high adiabatic wall temperature (or large forcing function); this makes the corrections for radiation and conduction along the body small compared with the large heat flow from the boundary to the skin. The results presented herein are an extension of the data shown in reference 4 for higher Mach numbers and different Reynolds number.

In order to obtain heat-transfer coefficients at high Mach numbers, measurements of skin temperatures have been made in flight tests conducted by the National Advisory Committee for Aeronautics on a parabolic body of revolution of fineness ratio 12.2. The model, known as the NACA RM-10, was rocket powered and fin stabilized. The tests were made at the Pilotless Aircraft Research Station at Wallops Island, Va.

The Mach number range covered in these tests was approximately 1.0 to 3.6. The Reynolds number range based on free-stream conditions and distance along the axis of the model from the nose to the measurement station was approximately 6×10^6 to 150×10^6. Heat-transfer data are presented for flight tests from four models.

SYMBOLS

A	surface area, sq ft
M	Mach number
V	velocity, ft/sec
h_e	local aerodynamic heat-transfer coefficient, Btu/(sec)(sq ft)($^\circ$F)
t	time, seconds from start of flight
c_p	specific heat of air at constant pressure, $\frac{\text{Btu/slug}}{^\circ\text{F}}$

ρ	density of air, slugs/cu ft
k	thermal conductivity of air, Btu/(sec)(sq ft)($^{\circ}$F/ft)
τ	wall thickness, ft
μ	viscosity of air, slugs/ft-sec
c_w	specific heat of wall material, $\frac{\text{Btu/lb}}{^{\circ}\text{F}}$
l	distance from the nose along the axis of the body, ft
γ_w	density of wall material, lb/cu ft
T	temperature, $^{\circ}$R
Nu	Nusselt number, dimensionless, $h_e l/k$
C_H	Stanton number, dimensionless, $h_e/c_p \rho V$
Pr	Prandtl number, dimensionless, $c_p \mu/k$
R	Reynolds number, dimensionless, $\rho V l/\mu$
RF	recovery factor
F	dimensionless parameter (ref. 12)
δ	boundary-layer thickness, ft
R_δ	Reynolds number, dimensionless, $\rho_v V_v \delta/\mu_v$
Nu_δ	Nusselt number, dimensionless, $h_e \delta/k_v$
C_f	average skin-friction coefficient
X	axial distance along model from maximum-diameter station, in.
Y	radius of model, in.
ϵ_1	emissivity of polished magnesium, 0.38
ϵ_2	emissivity of oxidized magnesium, 0.80

ϵ_r emissivity of oxidized aluminum, 0.18

σ Stefan-Boltzmann constant, 0.483×10^{-12} Btu/(sec)(sq ft)$(^{\circ}R)^4$

θ flight-path angle, deg

Subscripts:

o undisturbed free stream ahead of model

v outside the boundary layer

s isentropic stagnation

aw adiabatic wall

w condition of material pertaining to the skin of the test vehicle

r condition of material pertaining to the wall of the rocket motor

i incompressible

TEST VEHICLES

The general configuration of the RM-10 test vehicle is shown in figure 1. The body is basically a parabola of revolution having a maximum diameter of 12 inches and a fineness ratio of 15; however, the stern was cut off at 81.3 percent of full length to allow for the installation of the rocket motor. This resulted in an actual fineness ratio of 12.2. Four untapered stabilizing fins were equally spaced around the afterbody. They were swept back 60° with a total aspect ratio of 2.04 and had a 10-percent-thick circular-arc cross section normal to the leading edge. The design was chosen to attain a high degree of stability which insured testing near zero angle of attack.

The RM-10 test vehicle was designed for heat-transfer investigation. This was accomplished by minimizing the internal structure by maintaining sea-level pressure within the model during the flight. Figure 2 shows the internal construction of the models. The models were all metal and utilized spun magnesium-alloy skins. The thickness of the skin for each station at which temperature measurements were made is shown in table I. The surface roughness of the models was less than 60 microinches from peak to valley as measured by a Brush surface analyzer with a stylus of

0.0005-inch radius. The case of the rocket motor in the model has a temperature rise of approximately 50° F; estimates were made and it was found that this rise was not sufficient to affect the accuracy of the temperature measurements. Figure 3 is a photograph of the model and booster configuration on the launcher. The model is propelled by a two-stage propulsion system, the booster forming the first stage and the rocket motor within the model forming the second stage.

INSTRUMENTATION

Skin-temperature measurements were made by means of resistance-type thermometers cemented to the inner surface of the skin. These thermometers were made of fine platinum wire 0.0002 inch in diameter. Reference 5 gives a complete description and development of the temperature pickup.

The trajectory of the models was measured with an NACA modified SCR 584 radar theodolite and the flight velocity by a CW Doppler radar set as described in reference 6. Measurements of the atmosphere at the time of the tests were made with a standard radiosonde whose altitude was measured with the SCR 584 radar theodolite. A longitudinal accelerometer within the model was employed to extend the velocity measurements beyond the range of the Doppler radar. Data from the accelerometer and from the resistance temperature pickups were telemetered to a ground receiving station during the whole flight.

METHOD AND TESTS

The model was boosted to a Mach number of approximately 1.5 by a booster consisting of two 6.25-inch ABL Deacon rocket motors which separated from the model after burnout. A period of coasting followed, after which the 6.25-inch Deacon rocket motor carried internally in the model ignited and propelled the model to a Mach number of approximately 3.6. As a result of this staging arrangement, higher Mach numbers than those presented in reference 4 were obtained. The Deacon motors are described in reference 7.

The transient conditions of the test vehicles were particularly suited for obtaining aerodynamic heating and heat-transfer data because of the large heat flow to the body compared with other heat losses such as radiation and conduction along the body. The skin temperatures were continuously recorded by the resistance-type pickup and telemetered to a ground receiving station during the flight. From these data and from radiosonde observations, radar tracking, and the thermodynamic properties of the air and the skin, the heat-transfer coefficients were calculated.

The variation of Reynolds number per foot with Mach number, based on free-stream conditions, is shown in figure 4 for models A, B, C, and D.

Heat-transfer data for transient conditions at high Mach numbers such as were encountered during the flight tests of these vehicles is determined by making the following heat balance:

$$h_e A_w (T_{aw} - T_w) - A_w \sigma \epsilon_1 T_w^4 - A_w \sigma \frac{T_w^4 - T_r^4}{\frac{1}{\epsilon_r} + \frac{A_r}{A_w}\left(\frac{1}{\epsilon_2} - 1\right)} = c_w \gamma_w \tau_w A_w \frac{dT_w}{dt} \qquad (1)$$

The first term is the heat convected from the boundary layer to the skin. The radiation from the model to the atmosphere is given by the second term. The third term is the heat radiated from the internal surface of the model to the rocket motor by the method of reference 8. The heat absorbed by the skin is the right-hand side of the equation. The solar heat transfer was omitted because for the worst condition it had less than 2 percent effect on the heat-transfer coefficient. The thermodynamic properties of the air obtained from reference 9 were employed in reducing the data and are shown in figure 5. The specific heat of magnesium shown in figure 6 was obtained from reference 10. Every term in equation (1) is known except the adiabatic wall temperature T_{aw} and the heat-transfer coefficient h_e. In order to obtain T_{aw}, it is first necessary to determine the recovery factor.

The recovery factor is defined as the ratio of stagnation rise to the temperature just outside the boundary layer attained by an insulated wall. As the stagnation temperature outside the boundary layer is constant throughout the flow, the recovery factor may be written as

$$RF = \frac{T_{aw} - T_v}{T_s - T_v} \qquad (2)$$

If radiation and conduction were absent at the peak of the skin temperature, no heat would be transferred and the skin temperature and adiabatic wall temperature would coincide. For these tests, conduction along the skin was found to be negligible but radiation had a maximum effect of 2 percent on the recovery factor. To account for this, equation (1) was solved for $T_{aw} - T_w$ by assuming a value for the heat-transfer coefficient for the time of peak temperature.

By assuming that the measured recovery factor was constant throughout the flight, the adiabatic wall temperature was calculated for any

time throughout the flight by resolving equation (2), where

$$T_{aw} = RF\left(T_s - T_v\right) + T_v$$

The static and stagnation temperatures are known throughout the flight.

The heat-transfer coefficient is then calculated by resolving equation (1), where

$$h_e = \frac{c_w \gamma_w \tau_w \frac{dT_w}{dt} + \sigma \epsilon_1 T_w^4 + \frac{\left(T_w^4 - T_r^4\right)\sigma}{\frac{1}{\epsilon_r} + \frac{A_r}{A_w}\left(\frac{1}{\epsilon_2} - 1\right)}}{T_{aw} - T_w} \qquad (4)$$

and all other terms are as explained previously.

RESULTS AND DISCUSSION

Recovery Factor

Figure 7 presents the variation of skin temperature with time for a typical temperature measurement station. The skin temperature starts to increase during the boosting period and reaches a first maximum of approximately 150° F during the first coasting period. At 13 seconds, the sustainer rocket motor is ignited and thrusts for approximately 3.5 seconds, during which time the skin temperature starts to rise rapidly. A second peak temperature occurs at approximately 22.5 seconds, followed by a gradual decrease in skin temperature with time. At these peaks of skin temperature, the effects of surface conduction were calculated and found to be negligible. The measured skin temperature at the peak corrected for radiation is then equal to the adiabatic wall temperature, and, since the static and stagnation temperatures are known, the recovery factors can be calculated.

Measured recovery factors are shown in figure 8 plotted against longitudinal distance from the nose. Results for models A, B, C, and D are compared with the theories for laminar and turbulent flows, expressed as $Pr_w^{1/2}$ and $Pr_w^{1/3}$, respectively, based on wall temperature. These theoretical lines represent an average value of Prandtl number for wall temperatures between 600° R and 900° R. If the theoretical recovery factor were presented for each station or wall temperature, the theoretical

recovery factor would vary approximately 1 percent from the average line shown in figure 8. Recovery factors are presented for models A, B, C, and D. Despite this apparent indication of the presence of laminar flow on a recovery-factor basis, the heat-transfer data, as will be shown later, compared favorably with the results for turbulent heat transfer presented in reference 4. In addition, the Reynolds numbers for these stations were of a magnitude that would indicate that turbulent flow was present. As shown in figure 7, the stagnation temperature used in calculating the recovery factor varied rapidly with time. Therefore, the selection of the exact times at which the skin-temperature peaks occurred influenced the magnitude of the stagnation temperature used in the equation for recovery factor. The absence of sharply defined peaks in the curve for variation of skin temperature with time for some of the models contributed substantially to the scatter of the points shown in figure 8.

Heat Transfer

Although the measured recovery factors cannot be accepted as being the values characteristic of turbulent flow, the effect of small variations of recovery factor on the heat-transfer coefficient was small for most of the data presented. This can be seen from figure 7, since the heat-transfer potential used in calculating the coefficient was the difference in temperature between the wall and the adiabatic wall. A small change in recovery factor would cause a small change in the adiabatic wall temperature, and since the bulk of the data presented is for the time when the temperature potential is great (i.e., when values of $T_{aw} - T_w$ are large), the effect of any variation in recovery factor on the heat-transfer coefficient would be small. The flight data pertinent to the heat-transfer measurements is presented in table II for all models.

Correlation I

Model A.- Aerodynamic heat-transfer data obtained during the flight test of model A is presented in figure 9(a). The heat-transfer data for the six stations are correlated on a dimensionless basis of the Nusselt number divided by the cube root of the Prandtl number, expressed as a function of Reynolds number. The air properties are based on local flow conditions just outside the boundary layer. Correlation of previously published heat-transfer data (ref. 4) from investigations conducted on the RM-10 is indicated by the dashed line shown in figure 9. Despite the scatter apparent in the data, a new fairing of the data points for all models tested (solid line) does not differ markedly from the old. At high Reynolds numbers, the Mach number is also high and most of the data points are lower than the correlation, which indicates a possible reduction in heat transfer due to Mach number. It was impossible for

these test conditions to isolate any of the variables affecting the heat transfer such as Mach number, Reynolds number, and the heating condition T_w/T_v.

Models B, C, and D.- For clarity, models B, C, and D are shown in figure 9(b); however, the faired curve for the data is that for all four models. Heat transfer was measured at stations 85 and 117 for model B, and the values are correlated in the figure on the same dimensionless basis as was used for model A. The data are in agreement with the faired line from this investigation. As the Reynolds number decreased during the decelerating flight, the data crosses the line, so that at the lower Reynolds number for each station the heat transfer was higher than the line. As with model A, the line can be used to predict skin temperatures during the flight test with good accuracy.

The heat transfer for the 122-inch station on model C is presented in figure 9(b). Data points are presented for both coasting portions of the flight (flagged symbols are for first coast). The results indicate a reduction in the heat transfer of approximately 16 percent below the faired line during the second coasting period, whereas the first-coast results are approximately 10 percent higher than the faired line.

Station 18 on model D yielded heat-transfer data during the first coasting portion of its flight test which was approximately 12 percent higher than the faired line. During the second coast, the data correlated well with the line. It is of interest to note that the data taken at the same Reynolds number differ for the first and second coasting periods by approximately 20 percent for both models C and D. This suggests a Mach number effect, as the Mach number for model C for which data are presented varied from 1.43 to 1.14 for the first coast and 3.18 to 2.8 for the second coast. For model D the Mach number varied from 1.46 to 1.04 during the first coast and from 3.4 to 2.36 for the second coast. The ratio of T_w/T_v for both models is approximately 1.2 for the first coast and 1.8 for the second coast. For this variation of T_w/T_v the theory of reference 11 predicts only a small change in heat-transfer coefficient; however, the change corresponding to a Mach number change from 1.2 to 3.0 according to this theory is approximately 16 percent, which is in accord with the experimental results. Despite some possible effects of pressure gradient, it is felt that the significant change between the data for the first and second coasts is due to Mach number. A comparison of the skin temperature calculated from the faired line with the measured skin temperature for a typical flight test is shown in figure 10. The comparison is made for the flight conditions of station 125 of model A. The measured heat transfer for this station had approximately a 10 percent deviation from the faired line, which is shown to yield a maximum temperature difference of approximately 30° F. Within the Mach number and Reynolds number range of the flight tests, therefore,

the faired line would be sufficiently accurate for determining the skin temperature. It is felt that because these tests are for a higher Mach number than those of reference 4, and hence for a greater Mach number effect, the faired line of the data for this investigation would give more accurate heat-transfer coefficients over the Mach number range covered by these tests.

Correlation II

A theory for correlating the heat transfer in a compressible flow was presented in reference 12 which expressed the heat transfer as a function of Nusselt number, Reynolds number, Mach number, and surface temperature. The Mach number and temperature effects were incorporated in a factor F, which enables the theoretical heat transfer from a turbulent boundary layer having a 1/7-power velocity profile to be expressed by the equation

$$F \times Nu_{\delta} = 0.0225 R_{\delta}^{0.75}$$

The length term used in the Nusselt and Reynolds numbers was the boundary-layer thickness. Figure 11 presents the heat-transfer data for models A, B, and C on this basis. Models B and C which were, respectively, models 5 and 3 of the tests reported in reference 13, had a boundary-layer total-pressure rake located at stations 117 and 122, respectively, which yielded measured values of boundary-layer thickness. The boundary-layer thickness for station 125 on model A was obtained from a flight test of a similar model having the same trajectory. The boundary-layer thickness for stations 50, 68, 85, 100, and 110 on model A was determined by using reference 14 to obtain the variation of momentum thickness with axial distance, and relating the momentum thickness to the boundary-layer thickness according to reference 15. The data for all models are in agreement with the theoretical line. Because of the great amount of work involved in obtaining the boundary-layer thickness, the comparison with the theory is made only for the second coasting period.

In both methods of correlating the heat transfer, average scatter is of the order of 10 percent, indicating no distinct advantage in either correlation method. However, in calculating surface temperatures, the method of figure 9 is decidedly easier than that of figure 11 because of the necessity of determining the boundary-layer thickness in the latter method.

Reynolds Analogy

The interrelationship between skin friction and heat transfer, as expressed by the modified Reynolds analogy of reference 16, can be shown by the equation $C_H = 0.6C_F$ for surfaces subjected to flows having a Prandtl number of approximately 0.72. This equation was essentially constant over the Mach number range from $M = 0$ to $M = 5$. In conjunction with the heat-transfer program, skin-friction measurements have been made on six RM-10 bodies having approximately the same trajectory as the heat-transfer models (ref. 13). The skin-friction measurements were average values measured by means of a boundary-layer total-pressure rake installed at the 125-inch station. Consequently, an experimental comparison of the measured average skin friction and the average heat transfer could be made by utilizing the modified Reynolds analogy stated above to obtain average skin-friction coefficients. Model A of the current investigation had a sufficient longitudinal distribution of local heat-transfer coefficient to enable the integration of the local heat-transfer coefficient over the body surface area, thereby obtaining an average value. The average skin friction was then calculated by the modified Reynolds analogy. The results are shown in figure 12 as C_f/C_{f_i}, the ratio of the calculated average friction data of model A to the incompressible average skin-friction coefficients given in reference 17. The solid lines represent the results of the skin-friction investigation reported in reference 13, with each line corresponding to a particular temperature condition as expressed by the ratio $\frac{T_{aw} - T_w}{T_{aw} - T_v}$. Development of this heating parameter is discussed in reference 18. The value of the temperature parameter $\frac{T_{aw} - T_w}{T_{aw} - T_v}$ for model A, based on flow conditions at the station corresponding to the average surface area of the model, varied from 0.72 to -0.25. The heat-transfer data points are seen to possess the same trend with heating condition as that established by the solid lines, and in general are in good agreement with the results from the skin-friction investigation. This agreement indicates that the theoretical relationship of the Reynolds analogy as presented in reference 16 is in accordance with the experimental results.

CONCLUDING REMARKS

Experimental heat-transfer coefficients have been measured from flight tests of four parabolic bodies of revolution (NACA RM-10). The Mach numbers covered by the tests were from 1.0 to 3.6 and the Reynolds numbers were 6×10^6 to 150×10^6, based on axial distance from the nose to the stations where the skin temperature was measured.

The results indicate that although the measured recovery factors were lower than the theoretical turbulent recovery factor, the faired curve of the measured heat transfer agreed within 12 percent with the previously determined turbulent heat-transfer measurements made on two RM-10 models. These data, when correlated by use of a Nusselt, Prandtl, and Reynolds number relation, agreed with a faired line with a mean scatter of approximately 10 percent. The effect of this scatter on the skin temperature was shown by a comparison of the measured and calculated skin temperatures to yield an agreement within 30° F at peak temperature.

It was indicated that the difference between the heat-transfer data taken at approximately the same Reynolds number but at different Mach numbers was due primarily to the effect of Mach number on the heat transfer, rather than to the heating condition.

The heat-transfer data were also correlated with a theory by Donaldson for heat transfer in a compressible flow which utilized the boundary-layer thickness as the characteristic length in the Reynolds number and Nusselt number (NACA RM L52H04). The measured heat transfer had a mean scatter of approximately 10 percent from the theory.

The relation of heat transfer to skin friction was experimentally found to agree with the theoretical relationship established by Rubesin (NACA TN 2917), which stated that the Stanton number was equal to 0.6 of the skin-friction coefficient.

Langley Aeronautical Laboratory,
National Advisory Committee for Aeronautics,
Langley Field, Va., December 13, 1954.

REFERENCES

1. Eber, G. R.: Recent Investigation of Temperature Recovery and Heat Transmission on Cones and Cylinder in Axial Flow in the N.O.L. Aeroballistics Wind Tunnel. Jour. Aero. Sci., vol. 19, no. 1, Jan. 1952, pp. 1-6 and 14.

2. Scherrer, Richard: Comparison of Theoretical and Experimental Heat-Transfer Characteristics of Bodies of Revolution at Supersonic Speeds. NACA Rep. 1055, 1951. (Supersedes NACA RM A8L28 by Scherrer, Wimbrow, and Gowen; NACA TN 1975 by Wimbrow; NACA TN 2087 by Scherrer and Gowen; NACA TN 2131 by Scherrer; and NACA TN 2148 by Wimbrow and Scherrer.)

3. Fischer, W. W.: Supersonic Convective Heat Transfer Correlations From Skin-Temperature Measurements During Flights of V-2 Rockets No. 19 and No. 27. Rep. No. 55258, Gen. Elec. Co., July 1949.

4. Chauvin, Leo T., and deMoraes, Carlos A.: Correlation of Supersonic Convective Heat-Transfer Coefficients From Measurements of the Skin Temperature of a Parabolic Body of Revolution (NACA RM-10). NACA RM L51A18, 1951.

5. Fricke, Clifford L., and Smith, Francis B.: Skin-Temperature Telemeter for Determining Boundary-Layer Heat-Transfer Coefficients. NACA RM L50J17, 1951.

6. Morrow, John D., and Katz, Ellis: Flight Investigation at Mach Numbers From 0.6 to 1.7 To Determine Drag and Base Pressures on a Blunt-Trailing-Edge Airfoil and Drag of Diamond and Circular-Arc Airfoils at Zero Lift. NACA RM L50E19a, 1950.

7. Anon.: Jato Manual. SPIA/M1, The Johns Hopkins Univ., Appl. Phys. Lab., March 1949.

8. Jakob, Max, and Hawkins, George A.: Elements of Heat Transfer and Insulation. Second ed., John Wiley & Sons, Inc., c.1942, 1950.

9. Keenan, Joseph H., and Kaye, Joseph: Thermodynamic Properties of Air Including Polytropic Functions. John Wiley & Sons, Inc., 1945.

10. Kelley, K. K.: Contributions to the Data on Theoretical Metallurgy. II. High-Temperature Specific-Heat Equations for Inorganic Substances. Bulletin 371, Bur. Mines, 1934, p. 32.

11. Van Driest, E. R.: Turbulent Boundary Layer in Compressible Fluids. Jour. Aero. Sci., vol. 18, no. 3, Mar. 1951, pp. 145-160, 216.

12. Donaldson, Coleman duP.: Heat Transfer and Skin Friction for Turbulent Boundary Layers on Heated or Cooled Surfaces at High Speeds. NACA RM L52H04, 1952.

13. Loposer, J. Dan, and Rumsey, Charles B.: Flight Measurements of Average Skin-Friction Coefficients on a Parabolic Body of Revolution (NACA RM-10) at Mach Numbers From 1.0 to 3.7. NACA RM L54G14, 1954.

14. Rubesin, Morris W., Rumsey, Charles B., and Varga, Steven A.: A Summary of Available Knowledge Concerning Skin Friction and Heat Transfer and Its Application to the Design of High-Speed Missiles. NACA RM A51J25a, 1951.

15. Tucker, Maurice: Approximate Turbulent Boundary-Layer Development in Plane Compressible Flow Along Thermally Insulated Surfaces With Application to Supersonic-Tunnel Contour Correction. NACA TN 2045, 1950.

16. Rubesin, Morris W.: A Modified Reynolds Analogy for the Compressible Turbulent Boundary Layer on a Flat Plate. NACA TN 2917, 1953.

17. Von Kármán, Th.: Turbulence and Skin Friction. Jour. Aero. Sci., vol. 1, no. 1, Jan. 1934, pp. 1-20.

18. Maloney, Joseph P.: Drag and Heat Transfer on a Parabolic Body of Revolution (NACA RM-10) in Free Flight to Mach Number 2 With Both Constant and Varying Reynolds Number and Heating Effects on Turbulent Skin Friction. NACA RM L54D06, 1954.

TABLE I.- SKIN THICKNESS AND LOCATION OF MEASUREMENT STATIONS

Model	Station, in.	Skin thickness, in.
D	18	0.0845
A	50	.0906
A	68	.0906
A	85	.0906
B	85	.098
A	100	.084
A	110	.084
B	117	.104
C	122	.092
A	125	.084

TABLE II.- SUMMARY OF PRESENTED HEAT-TRANSFER DATA

Station, in.	Time, sec	M_0	T_{t_0}, °R	$T_{s_{t_0}}$, °R	V_0, ft/sec	ρ_0, slugs/cu ft	T_w, °R	V_w, ft/sec	ρ_w, slugs/cu ft	M_w	$T_{s_{t_w}}$, °R	q_w, Btu/ft²-sec	$\frac{dT_w}{d\tau}$, °F/sec	h_0	δ_1, ft	Re_1	Re_θ	F	$Pr^{1/3}$	x	R_θ	$F \times Re_\theta$	$\frac{Nu}{Pr^{1/3}}$
Model A																							
30	4	1.47	580.6	744.7	1,644	2.045×10^{-3}	525.7	1,635	2.076×10^{-3}	1.45	716.0	581.4	80.4	0.0530	———	3.32×10^4	———	———	0.896	37.4×10^6	———	———	3.81×10^4
	8	1.19	508.8	644.0	1,504	1.725	504.4	1,498	1.737	1.18	625.9	617.3	2.1	.0408	———	3.08	———	———	.897	85.4	———	———	3.38
	11	1.05	482.5	596.2	1,117	1.544	493.4	1,113	1.548	1.02	582.8	613.0	-3.5	.0658	———	2.80	———	———	.898	19.9	———	———	3.19
	17	3.68	441.4	1,696.5	3,795	1.047	465.2	3,774	1.194	3.54	1,487.6	880.9	86.8	.0516	0.0156	3.56	1.34×10^4	1.48	.900	53.7	2.01×10^5	1.99×10^4	3.86
	18.5	3.47	419.3	1,468.5	3,487	.880	439.4	3,454	.937	3.35	1,302.9	986.5	40.8	.0358	———	3.07	———	———	.900	42.7	———	———	3.40
	20	3.31	397.2	1,266.0	3,254	.748	414.4	3,201	.691	3.21	1,197.8	966.7	25.5	.0307	.0139	2.99	.86	1.55	.902	34.9	1.16	1.32	2.87
	22	3.18	378.0	1,113.0	2,973	.594	392.5	2,947	.651	3.08	1,021.5	981.9	1.6	.0265	———	8.12	———	———	.903	29.2	———	———	2.93
	24	2.90	378.2	1,015.2	2,769	.455	390.5	2,742	.495	2.88	953.9	980.4	-6.8	.0233	.008	1.73	.33	1.47	.903	18.6	.33	.48	1.964
	27.8	2.58	382.3	890.5	2,479	.285	391.6	2,457	.301	2.59	868.0	961.4	-6.1	.0096	.0232	1.26	.70	1.45	.905	10.1	.56	1.01	1.40
68	4	1.47	580.6	744.7	1,644	2.045	518.0	1,632	2.064	1.48	717.3	573.4	19.9	.0891	———	4.12	———	———	.896	30.7	———	———	4.60
	8	1.19	508.8	644.0	1,504	1.725	500.8	1,517	1.702	1.20	626.6	606.0	2.2	.0650	———	3.30	———	———	.897	69.5	———	———	3.68
	11	1.05	482.5	596.2	1,117	1.544	489.7	1,130	1.582	1.04	589.3	605.2	-0.1	.0195	———	2.89	———	———	.898	27.2	———	———	3.22
	17	3.68	441.4	1,696.5	3,795	1.047	450.7	3,776	1.107	3.62	1,497.5	789.5	79.7	.0681	.0959	4.48	2.74	1.51	.901	69.7	4.85	4.19	4.97
	18.5	3.47	419.3	1,468.5	3,487	.880	426.2	3,473	.928	3.42	1,277.2	870.8	33.6	.0414	———	3.54	———	———	.902	56.1	———	———	3.95
	20	3.31	397.2	1,266.0	3,254	.748	405.1	3,222	.725	3.27	1,133.7	907.5	16.3	.0372	.0356	2.99	1.77	1.56	.903	45.5	3.69	2.75	3.51
	22	3.18	378.0	1,113.0	2,973	.594	382.3	2,966	.611	3.09	1,002.7	927.3	4.9	.0332	———	2.59	———	———	.904	34.1	———	———	2.65
	24	2.90	378.2	1,015.2	2,769	.455	381.2	2,763	.465	2.88	919.5	929.8	-1.2	.0300	.0294	1.82	.94	1.52	.904	24.3	1.87	1.43	2.98
	27.8	2.58	382.3	890.5	2,479	.285	383.5	2,477	.285	2.57	874.8	920.0	-3.4	.0066	.0597	1.19	.84	1.48	.904	13.4	.94	1.24	1.32
85	4	1.47	580.6	744.7	1,644	2.045	514.3	1,667	1.988	1.50	685.8	568.4	17.6	.0835	———	3.96	———	———	.897	62.8	———	———	6.63
	8	1.19	508.8	644.0	1,504	1.725	497.8	1,550	1.680	1.61	605.4	597.9	.9	.0608	———	4.17	———	———	.898	45.2	———	———	4.65
	11	1.05	482.5	596.2	1,117	1.544	486.0	1,140	1.569	1.05	567.7	595.2	-2.0	.0184	———	3.05	———	———	.898	24.1	———	———	3.40
	17	3.68	441.4	1,696.5	3,795	1.047	454.8	3,805	1.080	3.78	1,432.3	765.1	64.1	.0819	.0549	4.50	3.47	1.54	.901	82.0	6.35	5.37	5.00
	18.5	3.47	419.3	1,468.5	3,487	.880	418.6	3,492	.893	3.51	1,256.1	835.8	30.2	.0185	———	3.88	———	———	.902	66.5	———	———	4.51
	20	3.31	397.2	1,266.0	3,254	.748	390.5	3,262	.719	3.33	1,117.5	869.1	16.0	.0154	.0585	3.44	2.59	1.59	.903	54.5	4.05	4.03	3.81
	22	3.18	378.0	1,113.0	2,973	.594	371.4	2,988	.571	3.16	987.2	888.6	4.8	.0122	———	2.83	———	———	.903	41.5	———	———	3.13
	24	2.90	378.2	1,015.2	2,769	.455	371.4	2,789	.496	2.94	905.7	891.1	-1.2	.0096	.0489	2.88	1.55	1.55	.903	29.5	2.01	2.40	2.98
	27.8	2.58	382.3	890.5	2,479	.285	373.4	2,496	.471	2.62	863.4	883.3	-2.4	.0062	.0558	1.49	1.11	1.49	.904	16.5	1.28	1.69	1.58
100	4	1.47	580.6	744.7	1,644	2.045	518.4	1,674	1.988	1.51	709.9	574.0	19.2	.0868	———	5.60	———	———	.897	73.6	———	———	6.85
	8	1.19	508.8	644.0	1,504	1.725	496.4	1,555	1.670	1.62	661.9	606.1	1.4	.0194	———	4.11	———	———	.898	50.8	———	———	4.59
	11	1.05	482.5	596.2	1,117	1.544	486.9	1,145	1.489	1.06	579.8	602.1	-3.2	.0158	———	3.45	———	———	.898	40.0	———	———	3.85
	17	3.68	441.4	1,696.5	3,795	1.047	417.5	3,885	.965	3.78	1,451.0	775.9	63.5	.0196	.0727	4.87	4.41	1.56	.902	95.2	8.47	6.98	5.41
	18.5	3.47	419.3	1,468.5	3,487	.880	401.6	3,518	.795	3.58	1,272.4	849.3	36.4	.0174	———	4.45	———	———	.903	74.6	———	———	4.94
	20	3.31	397.2	1,266.0	3,254	.748	381.8	3,269	.679	3.41	1,131.5	887.7	16.7	.0151	.0717	4.02	3.44	1.61	.904	61.9	5.34	5.54	4.45
	22	3.18	378.0	1,113.0	2,973	.594	368.6	3,004	.640	3.21	999.1	905.5	4.2	.0122	———	3.38	———	———	.905	46.8	———	———	3.74
	24	2.90	378.2	1,015.2	2,769	.455	364.7	2,796	.617	2.98	916.5	909.1	-.4	.0096	.0676	2.67	2.16	1.57	.905	33.6	2.73	3.40	2.95
	27.8	2.58	382.3	890.5	2,479	.285	370.2	2,509	.359	2.69	818.5	900.5	-3.4	.0058	.0725	1.59	1.57	1.51	.905	18.6	1.62	2.08	1.76
110	17	3.68	441.4	1,696.5	3,795	1.047	414.3	3,837	.909	3.84	1,419.1	779.3	65.6	.0808	.0951	5.56	5.65	1.57	.903	100.6	10.82	8.86	6.16
	18.5	3.47	419.3	1,468.5	3,487	.880	399.2	3,531	.760	3.62	1,263.8	848.0	36.6	.0160	———	4.37	———	———	.903	80.0	———	———	5.06
	20	3.31	397.2	1,266.0	3,254	.748	378.7	3,273	.656	3.44	1,106.4	882.7	15.0	.0129	.0882	3.88	3.68	1.61	.904	66.7	6.43	5.93	4.86
	22	3.18	378.0	1,113.0	2,973	.594	358.9	3,014	.622	3.09	977.1	881.2	4.9	.0093	———	3.04	———	———	.903	50.5	———	———	3.36
	24	2.90	378.2	1,015.2	2,769	.455	360.8	2,806	.406	2.81	896.8	888.0	-.1	.0074	.0889	2.89	2.08	1.57	.903	36.9	3.34	3.87	2.99
	27.8	2.58	382.3	890.5	2,479	.285	367.2	2,515	.357	2.67	796.4	880.0	-1.6	.0059	.0859	1.19	1.11	1.52	.903	20.5	1.98	1.69	1.38
125	4	1.47	580.6	744.7	1,644	2.045	510.4	1,685	1.949	1.51	708.5	566.3	16.4	.0828	———	5.98	———	———	.897	82.2	———	———	6.67
	8	1.19	508.8	644.0	1,504	1.725	493.7	1,558	1.663	1.62	617.5	598.2	2.0	.0182	———	4.34	———	———	.898	63.5	———	———	5.12
	11	1.05	482.5	596.2	1,117	1.544	486.7	1,147	1.494	1.06	576.5	597.0	-1.6	.0169	———	4.62	———	———	.898	50.1	———	———	5.15
	17	3.68	441.4	1,696.5	3,795	1.047	404.8	3,852	.845	3.90	1,464.7	759.8	58.1	.0196	.1264	5.83	7.35	1.59	.903	108.5	15.35	12.00	6.68
	18.5	3.47	419.5	1,468.5	3,487	.880	387.4	3,541	.734	3.67	1,881.7	827.0	34.8	.0159	———	5.86	———	———	.903	88.5	———	———	6.63
	20	3.31	397.2	1,266.0	3,254	.748	368.7	3,287	.684	3.49	1,139.5	865.9	15.5	.0139	.1195	4.42	5.08	1.65	.903	73.5	13.3	8.27	4.89
	22	3.18	378.0	1,113.0	2,973	.594	353.4	3,015	.504	3.28	1,005.9	882.8	5.2	.0100	———	3.57	———	———	.903	56.2	———	———	3.94
	24	2.90	378.2	1,015.2	2,769	.455	356.2	2,816	.392	3.04	922.5	888.4	1.0	.0080	.1185	2.84	3.06	1.59	.903	40.7	4.86	4.86	3.13
	27.8	2.58	382.3	890.5	2,479	.285	365.8	2,524	.290	2.69	827.1	885.3	-2.3	.0058	.1145	1.85	2.03	1.58	.903	22.9	2.51	3.10	2.04

TABLE II.- SUMMARY OF PRESENTED HEAT-TRANSFER DATA - Concluded

Station, in.	Time, sec	M_0	T_{t_0}, °R	T_{s_0}, °R	V_0, ft/sec	ρ_0, slugs/cu ft	T_{t_1}, °R	V_1, ft/sec	ρ_1, slugs/cu ft	M_1	T_{aw}, °R	T_{t_2}, °R	$\frac{dT_{t_2}}{dt}$, °F/sec	h_0	x_t, ft	Re_1	Re_b	F	$Pr^{1/3}$	B	R_b	F × R_b	$\frac{St}{Pr^{1/3}}$
Model B																							
85	12	3.45	489.8	1,656.4	3,733	1.559×10^{-3}	482.1	3,767	1.512×10^{-3}	3.49	1,587.2	735.0	90.9	0.0279	——	5.21×10^4	——	——	0.899	114.0×10^6	——	——	5.80×10^4
	14	2.97	489.8	1,341.6	3,807	1.334	477.4	3,882	1.279	3.01	1,446.5	679.5	35.6	.0227	——	4.86	——	——	.899	89.2	——	——	4.74
	16	2.63	472.2	1,189.3	3,807	1.149	465.8	3,884	1.148	2.67	1,092.5	919.8	9.3	.0197	——	3.80	——	——	.900	66.9	——	——	4.21
	20	2.16	450.0	869.9	3,857	.931	448.4	3,876	.939	2.19	822.9	918.4	-2.3	.0160	——	3.21	——	——	.901	46.6	——	——	3.96
	28	1.87	450.3	731.7	1,981	.857	423.9	1,941	.886	1.91	702.5	873.7	-10.8	.0139	——	2.88	——	——	.902	35.9	——	——	3.80
	30	1.62	410.6	686.7	1,613	.732	409.1	1,655	.707	1.65	608.3	808.5	-11.5	.0121	——	2.61	——	——	.903	26.6	——	——	2.89
117	12	3.45	489.8	1,656.4	3,733	1.559	456.3	3,806	1.508	3.64	1,548.4	742.1	85.3	.0264	0.0918	7.11	6.69×10^4	1.48	.900	143.4	13.57×10^6	9.54×10^6	7.91
	14	2.97	489.8	1,341.6	3,807	1.334	458.6	3,856	1.188	3.11	1,262.1	693.0	55.5	.0220	——	6.02	——	——	.900	108.0	——	——	6.59
	16	2.63	472.2	1,189.3	3,807	1.195	450.1	3,883	1.099	2.73	1,064.5	699.8	18.2	.0199	.1033	5.43	5.73	1.45	.900	88.6	9.81	8.84	6.04
	20	2.16	450.0	869.9	3,857	.991	434.1	3,897	.906	2.24	830.7	905.7	-6.3	.0162	.1029	4.35	4.78	1.41	.901	68.8	6.41	6.74	5.05
	24	1.87	450.3	731.7	1,981	.897	417.9	1,977	.797	1.96	708.0	871.7	-8.9	.0131	.1105	3.79	4.39	1.38	.903	48.5	5.47	6.09	4.80
	30	1.62	410.6	686.7	1,613	.734	400.8	1,645	.690	1.68	606.4	816.0	-9.8	.0114	.1185	3.42	3.95	1.35	.903	36.3	4.11	5.34	3.79
Model C																							
122	3.8	1.43	484.7	688.7	1,547	2.897	473.5	1,581	2.191	1.48	684.3	738.5	17.0	.0272	.0859	7.39	6.27	1.09	.899	100.4	8.80	6.88	8.82
	6.5	1.28	481.7	621.6	1,858	2.017	474.6	1,930	1.944	1.25	608.2	764.0	4.6	.0200	.0900	5.45	4.77	1.10	.899	74.7	6.98	5.25	6.04
	7.4	1.14	481.0	606.8	1,830	1.956	474.5	1,881	1.870	1.18	594.5	707.1	2.4	.0184	.0875	5.01	4.38	1.10	.899	68.3	5.85	4.73	5.37
	17.8	3.18	460.0	1,268.9	3,195	1.088	398.1	3,346	.918	3.34	1,196.1	789.8	34.3	.0162	.0891	5.14	4.54	1.46	.903	89.3	8.67	6.68	5.85
	20.6	2.82	397.5	1,081.5	2,761	.815	373.2	2,808	.706	2.96	977.0	786.7	9.2	.0118	.0855	3.69	3.02	1.46	.903	68.5	5.69	4.43	4.20
	25.5	2.45	401.2	897.6	2,443	.679	388.9	2,487	.526	2.59	854.8	797.8	1.7	.0085	.0891	2.70	2.36	1.44	.904	45.7	3.84	3.39	3.07
	30	2.09	386.6	784.9	2,017	.580	373.4	2,056	.494	2.17	695.7	791.4	-2.4	.0050	——	1.66	——	——	.905	21.0	——	——	1.69
Model D																							
18	3.5	1.46	494.4	706.0	1,596	2.318	507.1	1,548	2.460	1.46	673.7	549.5	30.3	.0458	——	1.78	——	——	.898	18.4	——	——	1.98
	5.0	1.30	495.5	670.7	1,457	2.166	504.3	1,411	2.287	1.34	644.0	581.5	13.1	.0399	——	1.52	——	——	.898	12.7	——	——	1.67
	8.0	1.14	497.8	626.3	1,264	1.956	496.2	1,203	2.045	1.15	597.5	596.8	-.5	.0350	——	1.27	——	——	.898	9.8	——	——	1.40
	10.0	1.04	487.0	595.7	1,152	1.888	494.5	1,091	1.899	1.08	578.1	593.0	-2.5	.0297	——	1.14	——	——	.899	8.3	——	——	1.27
	16.5	3.88	469.0	1,438.6	3,410	1.448	503.3	3,344	1.761	3.88	1,865.5	737.5	138.2	.0359	——	2.18	——	——	.900	25.2	——	——	2.43
	18.0	3.40	454.4	1,305.5	3,350	1.291	494.8	3,456	1.568	3.39	1,321.9	914.5	84.9	.0431	——	1.79	——	——	.900	22.0	——	——	1.99
	22.0	2.77	484.6	1,073.7	2,794	.978	451.9	2,755	1.144	2.76	961.8	1,005.8	-7.6	.0301	——	1.51	——	——	.902	13.4	——	——	1.46
	26.0	2.36	464.8	855.3	2,388	.776	485.2	2,436	.882	2.56	777.9	965.5	-18.0	.0218	——	1.00	——	——	.905	9.0	——	——	1.11
	30.0	2.10	395.9	755.0	2,019	.689	418.5	1,969	.696	2.08	677.0	879.5	-14.4	.0148	——	.70	——	——	.904	6.3	——	——	.77

CONFIDENTIAL

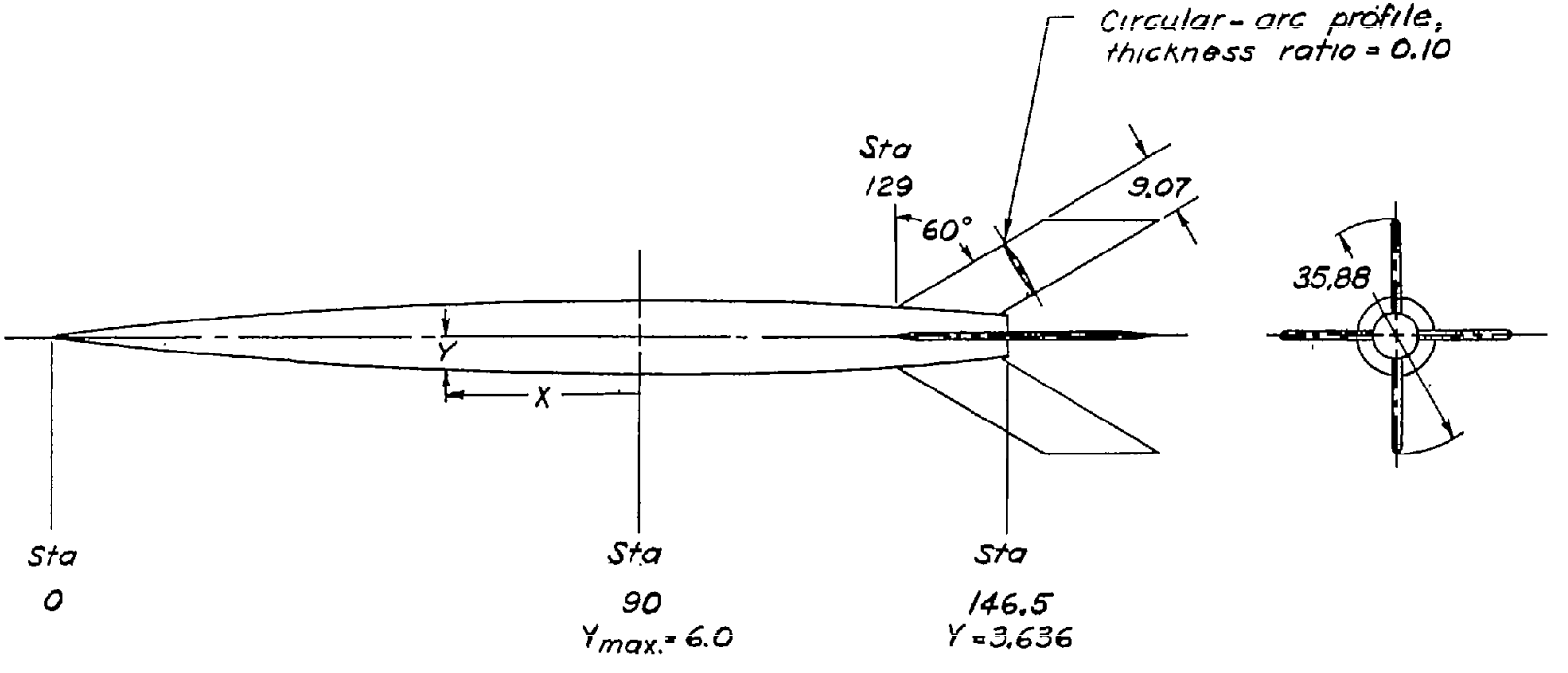

Figure 1.- General configuration of the NACA RM-10 model. Body profile equation, $Y = 6.000 - 0.0007407X^2$. Station numbers denote axial distance from nose in inches. Dimensions are in inches.

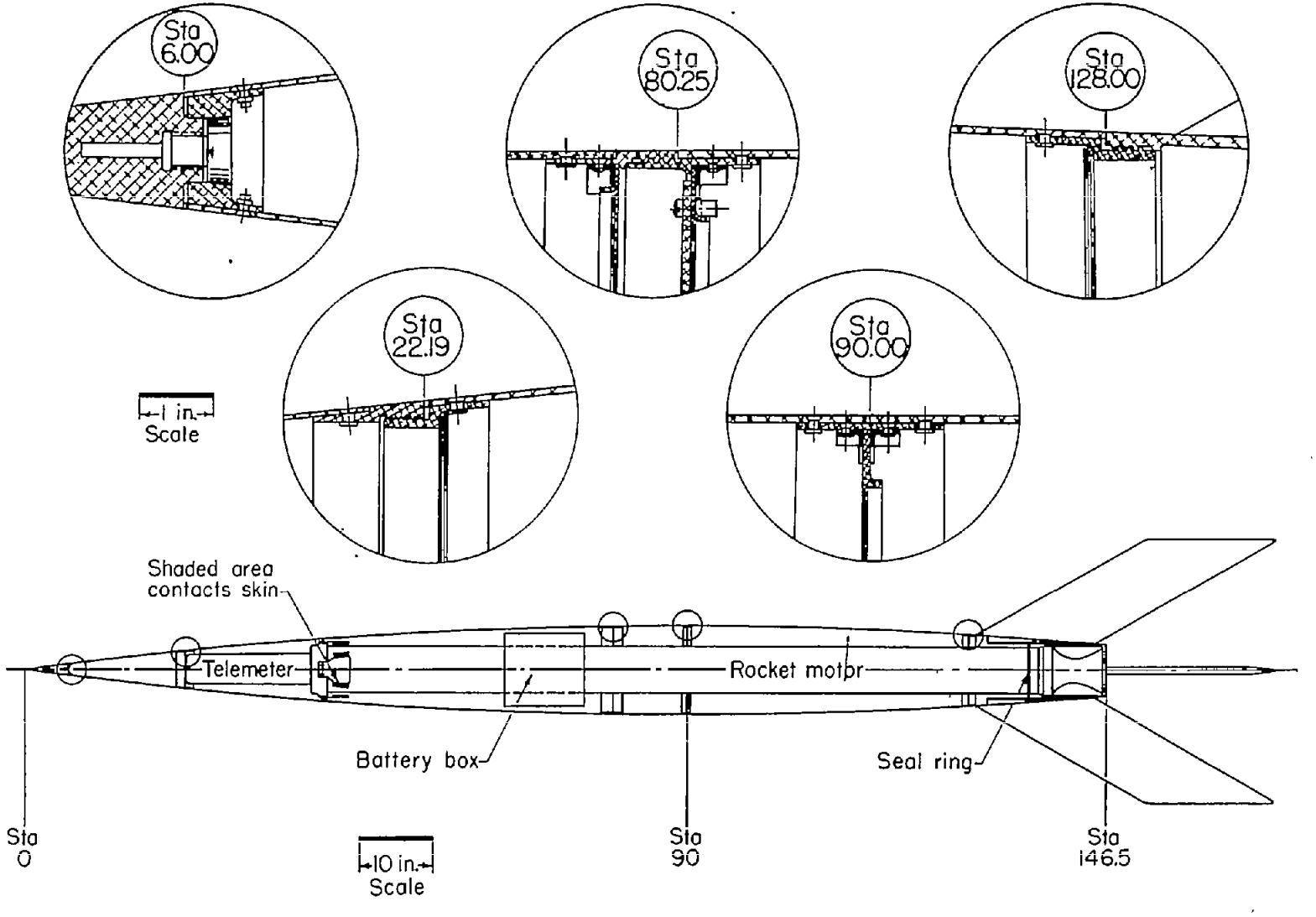

Figure 2.- Internal construction of the NACA RM-10 model.

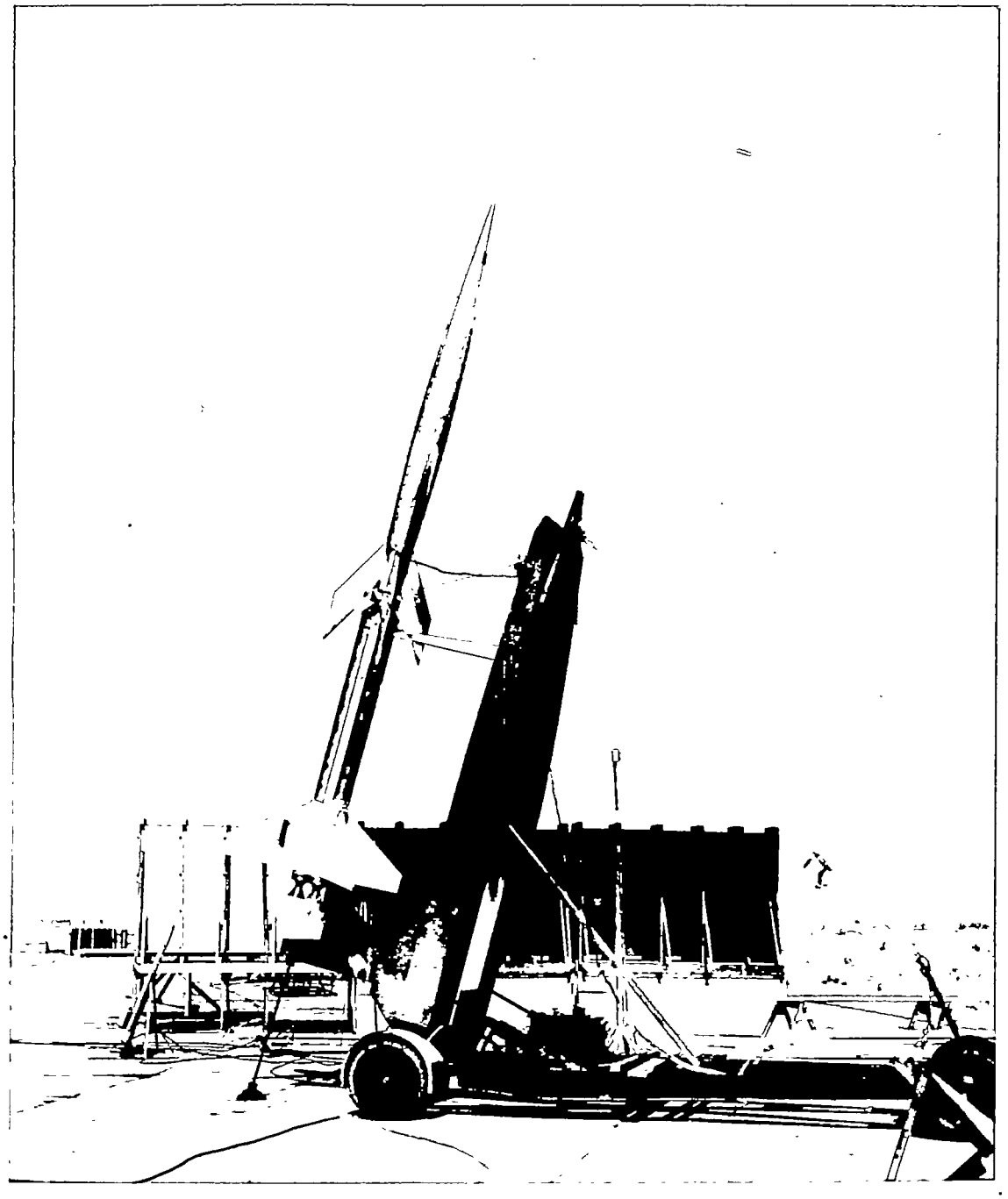

Figure 3.- Photograph of model and booster configuration. L-74852

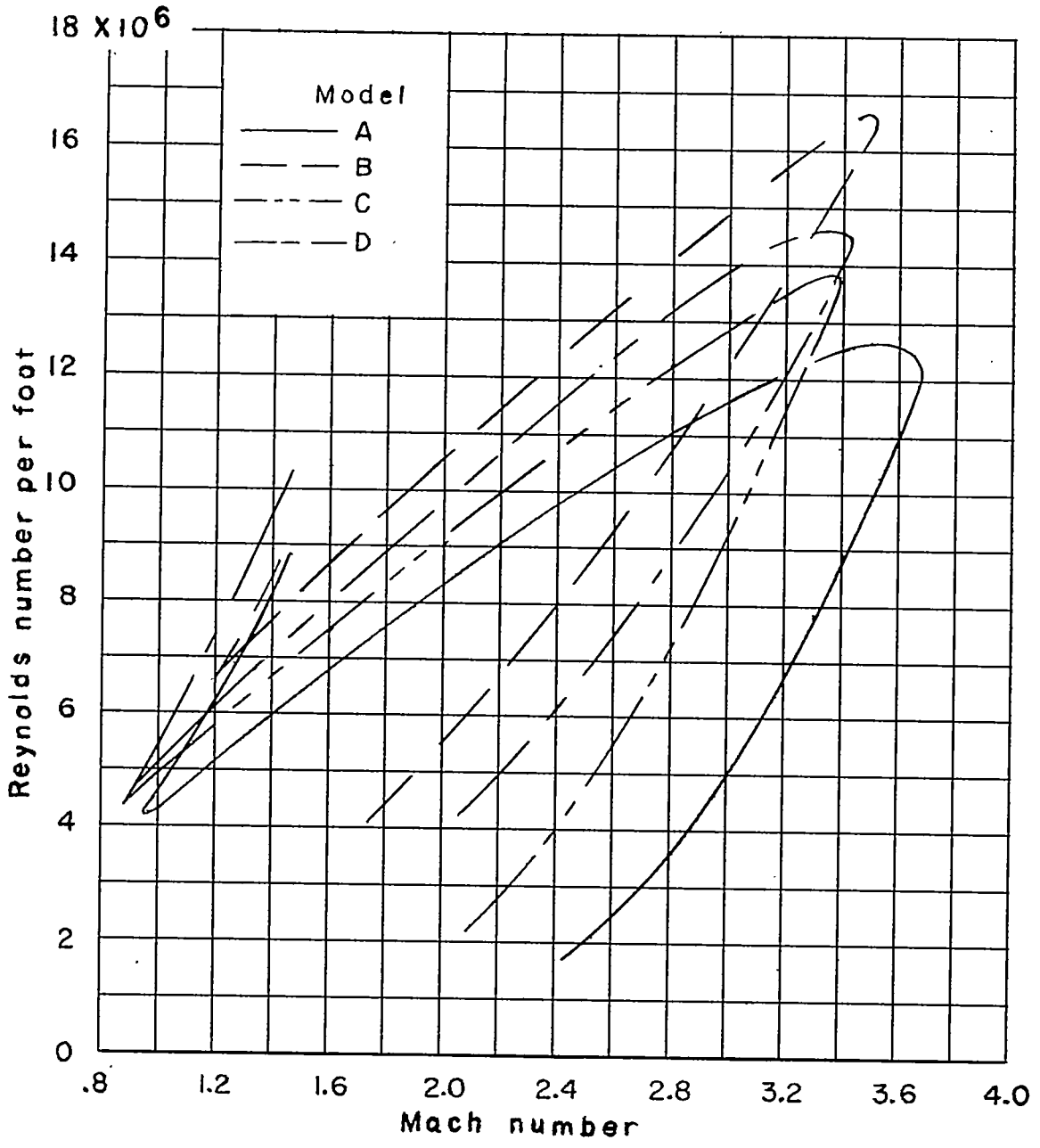

Figure 4.- Variation of the Reynolds number per foot with Mach number, obtained during four flight tests of a parabolic body of revolution (NACA RM-10).

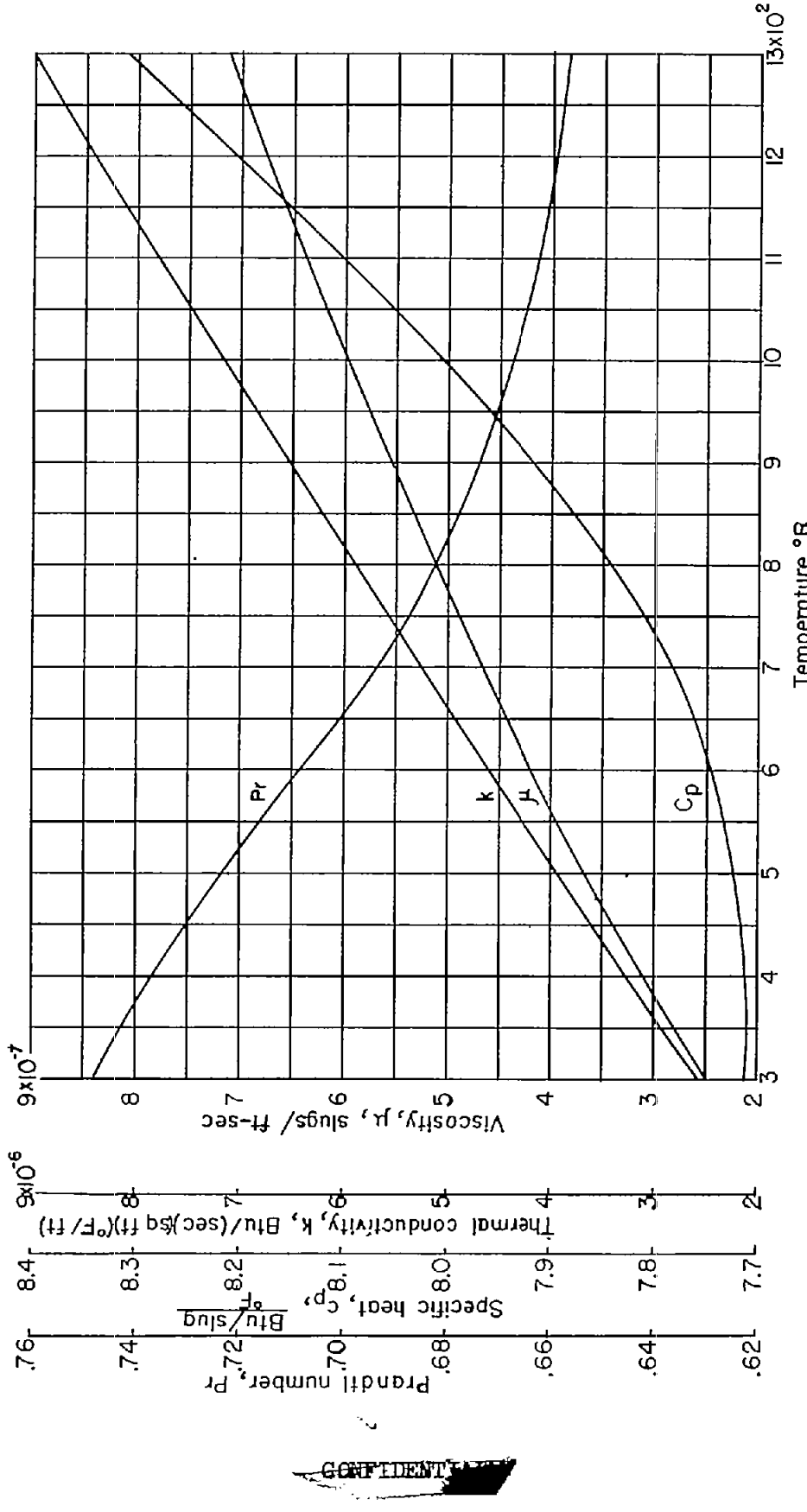

Figure 5.- Thermodynamic properties of air (ref. 9).

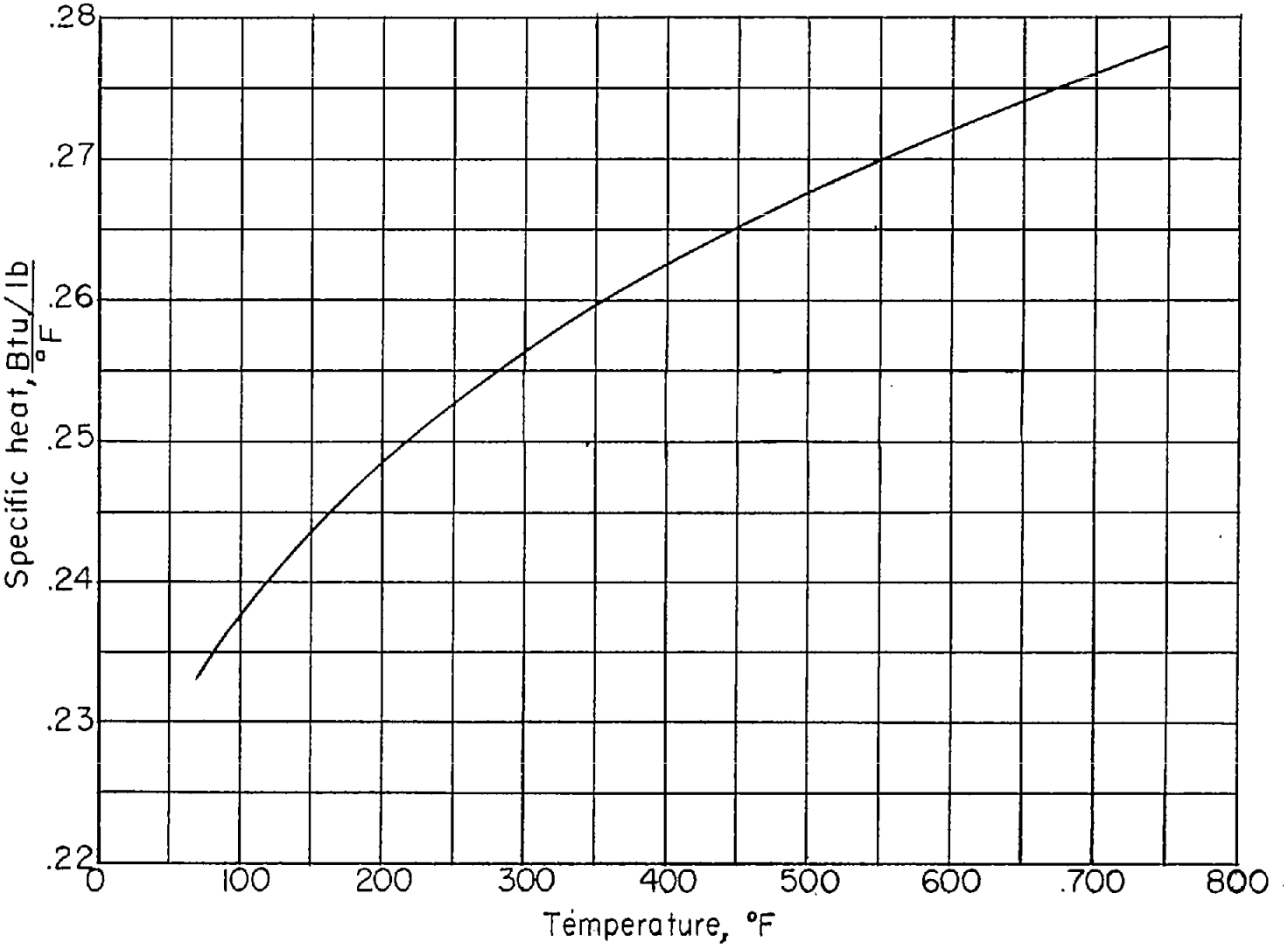

Figure 6.- Specific heat of magnesium.

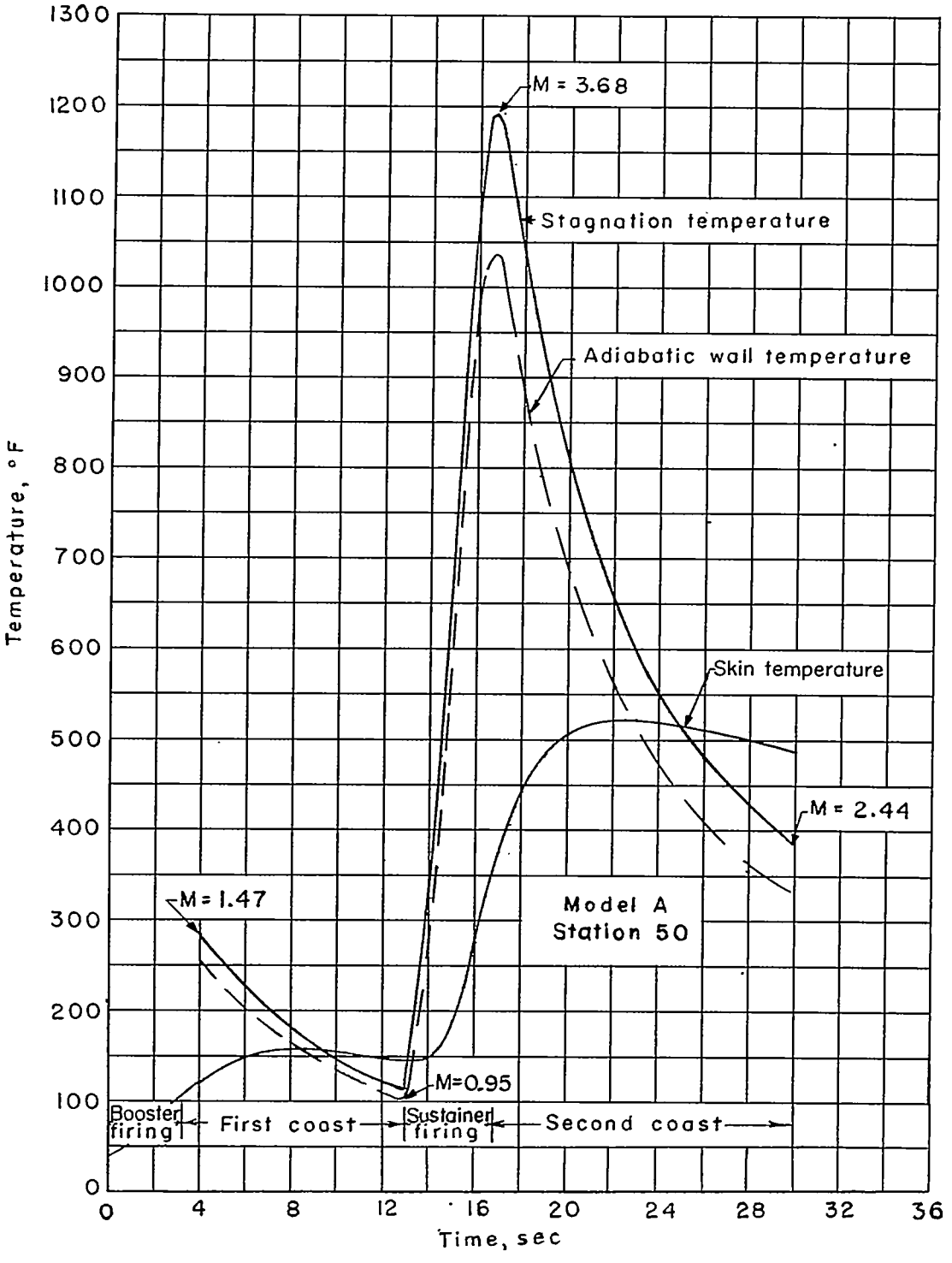

Figure 7.- Typical time history of stagnation, adiabatic, and skin temperatures obtained from a flight test of a parabolic body of revolution (NACA RM-10).

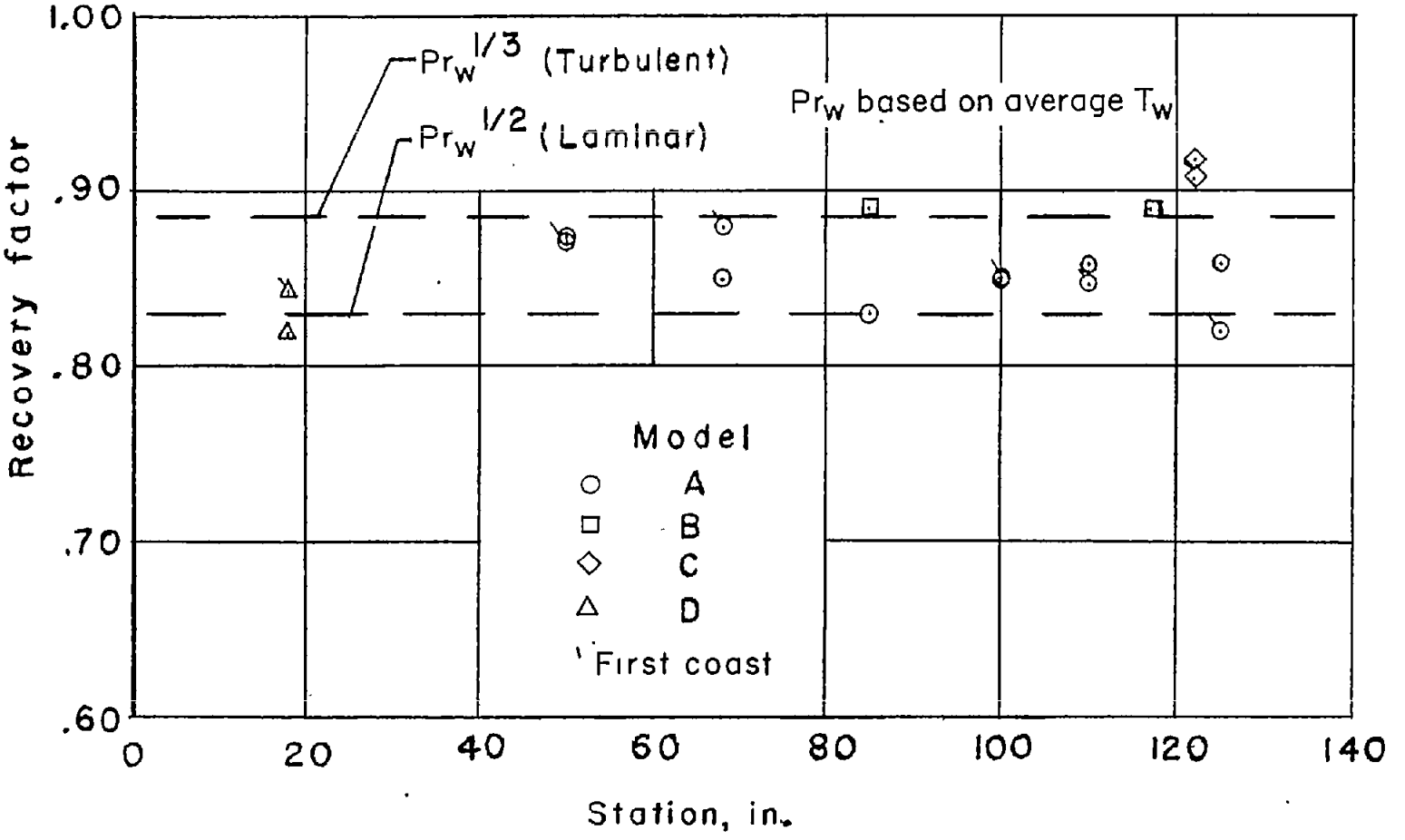

Figure 8.- Measured recovery factors obtained during flight tests.

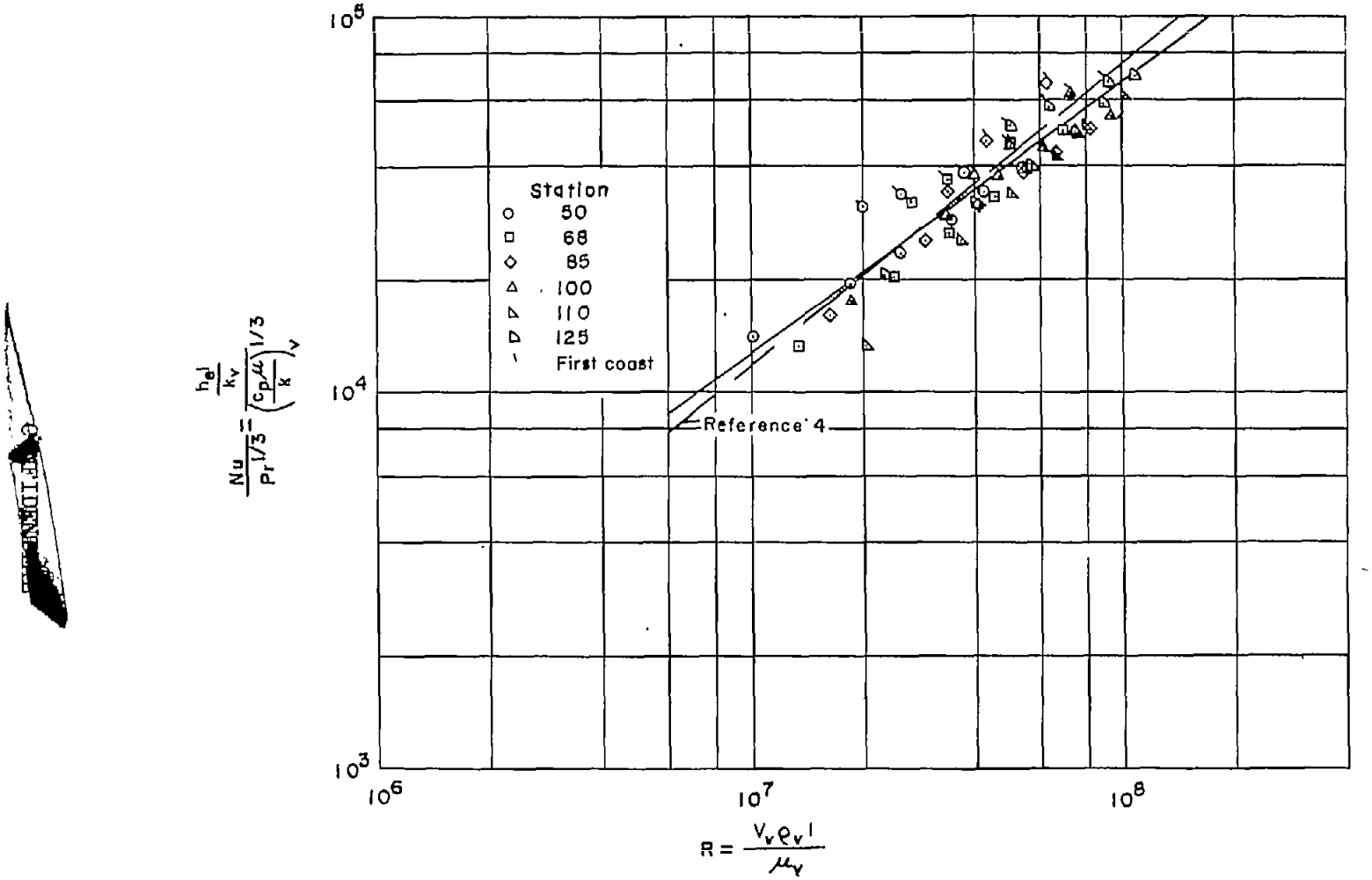

(a) Model A.

Figure 9.- Correlation of heat transfer from four flight tests.

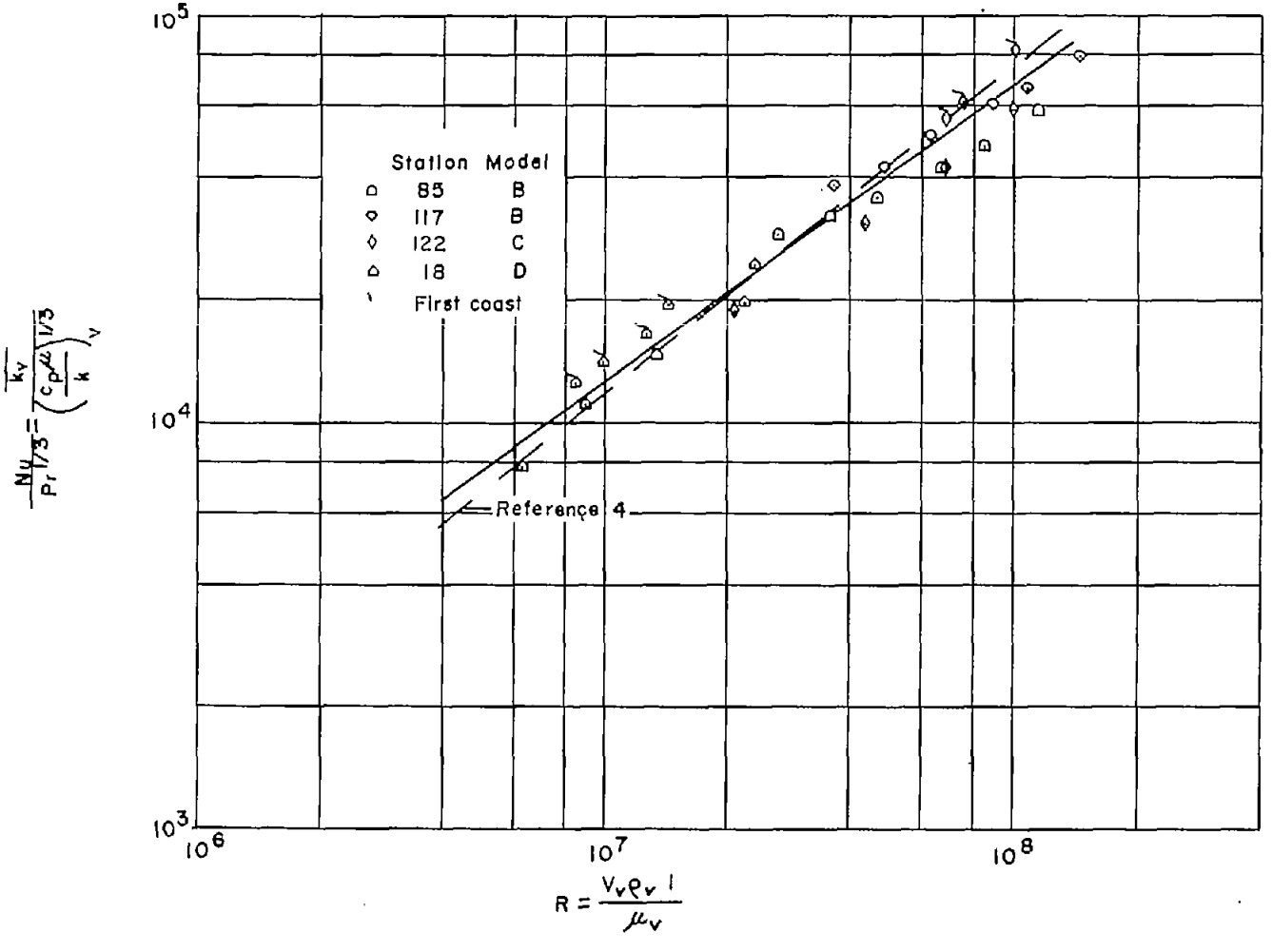

(b) Models B, C, and D.

Figure 9.- Concluded.

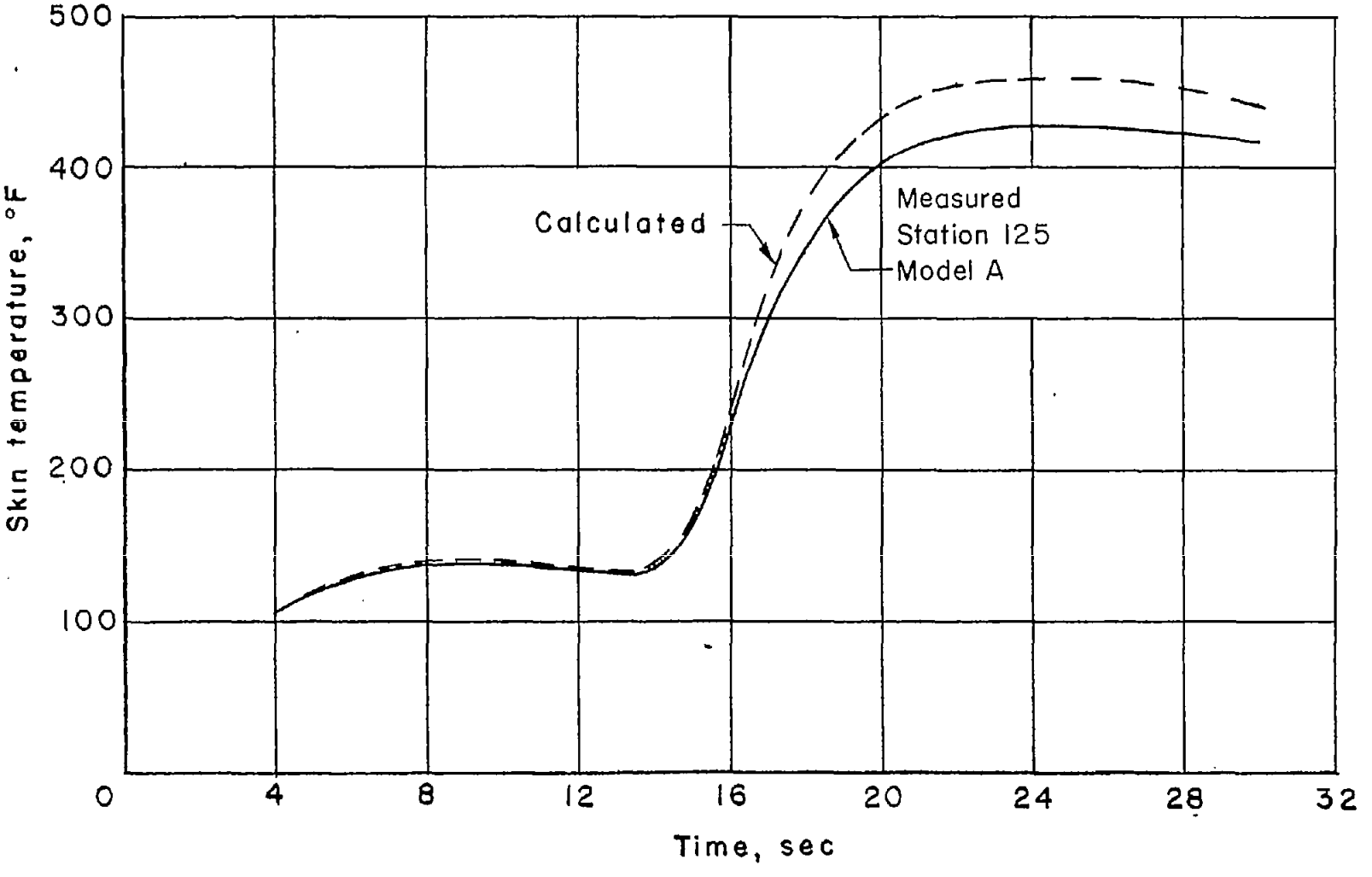

Figure 10.- Comparison of measured skin temperature with skin temperature calculated from faired line.

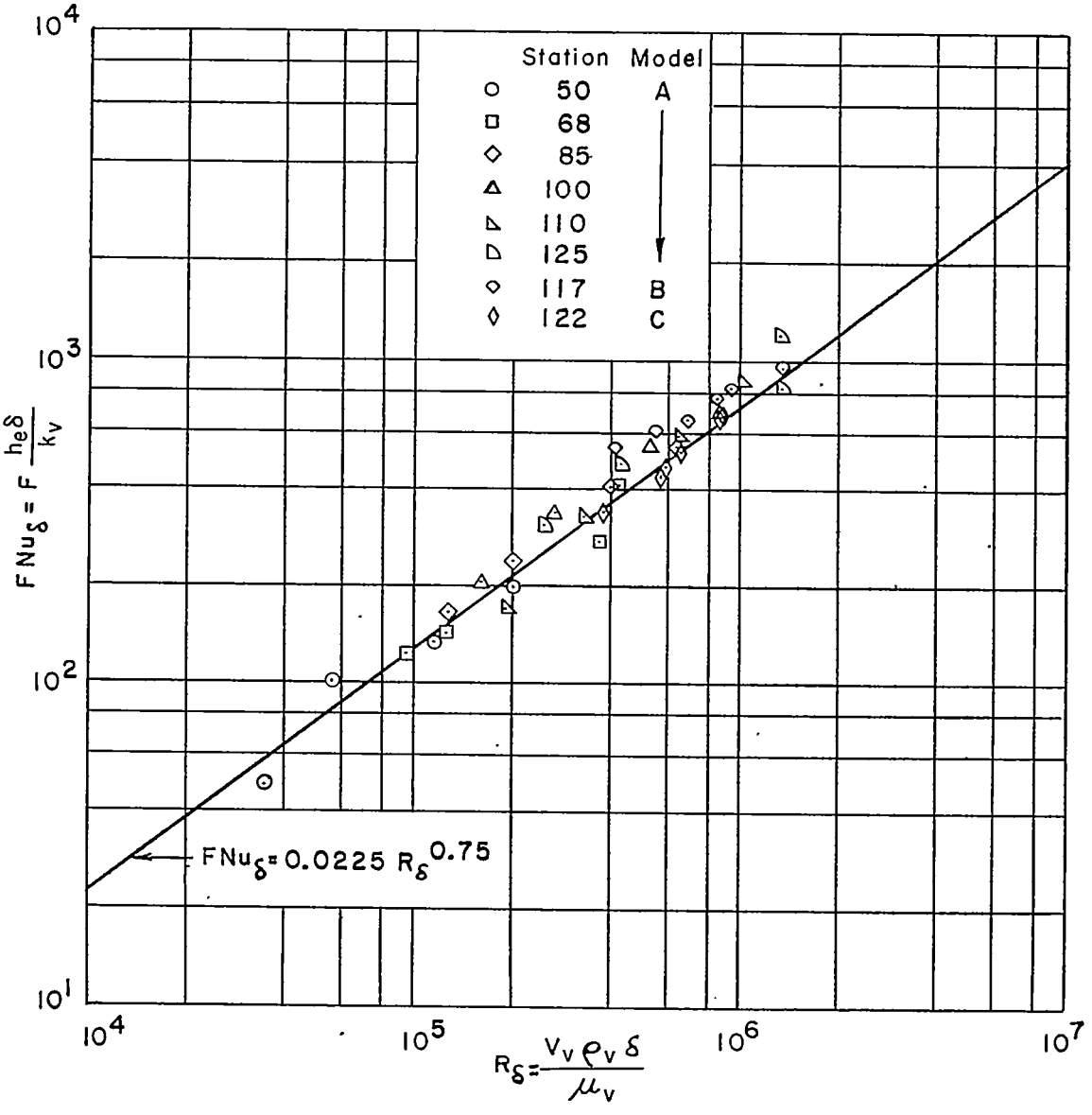

Figure 11.- Heat-transfer data obtained from flight tests A, B, and C and correlated with theory of reference 12.

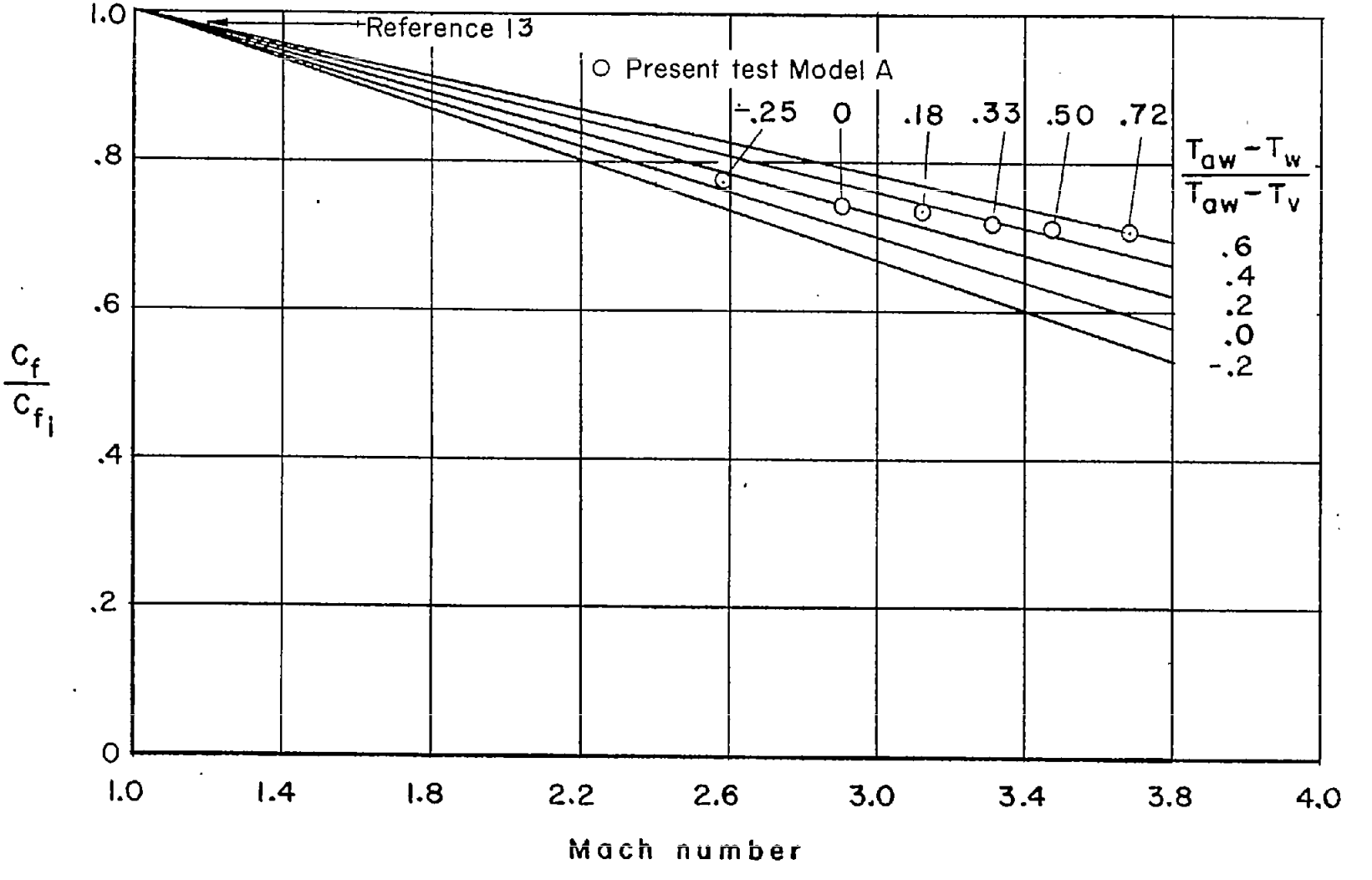

Figure 12.- Comparison of average skin friction calculated from modified Reynolds analogy with measured average skin friction.